Construction and Building Materials 68 (2014) 158–171

Contents lists available at ScienceDirect

Construction and Building Materials

journal homepage: www.elsevier.com/locate/conbuildmat

Static properties and impact resistance of a green Ultra-High Performance Hybrid Fibre Reinforced Concrete (UHPHFRC): Experiments and modeling

R. Yu *, P. Spiesz, H.J.H. Brouwers

Department of the Built Environment, Eindhoven University of Technology, P.O. Box 513, 5600 MB Eindhoven, The Netherlands

HIGHLIGHTS

- A green Ultra-High Performance Hybrid Fibre Reinforced Concrete is produced.
- Modified Andreasen & Andersen particle packing model is utilized.
- Effect of hybrid steel fibres on the workability of UHPHFRC is investigated.
- Impact resistance of UHPHFRC is tested and analyzed.
- Energy absorption process of UHPHFRC under impact is analyzed and modeled.

ARTICLE INFO

Article history:
Received 1 April 2014
Received in revised form 18 June 2014
Accepted 19 June 2014

Keywords:
Ultra-High Performance Hybrid Fibre Reinforced Concrete (UHPHFRC)
Green
Static properties
Impact resistance
Modeling

ABSTRACT

This paper addresses the static properties and impact resistance of a "green" Ultra-High Performance Hybrid Fibre Reinforced Concrete (UHPHFRC). The design of concrete mixtures aims to achieve a densely compacted cementitious matrix, employing the modified Andreasen & Andersen particle packing model. The flowability, static mechanical properties and impact resistance capacity of UHPHFRC are measured and analyzed. The results show that by utilizing the improved packing model, it is possible to design a type of UHPHFRC with a relatively low binder amount, which can make the concrete more "green". Moreover, due to the mutual effect between the long and short steel fibres, the hybrid fibre reinforced concrete shows better workability and higher static mechanical properties. Nevertheless, the impact resistance capacity of UHPHFRC is dominated by the long steel fibres. Additionally, the energy absorption process of UHPHFRC under dynamic loading is analyzed and modeled.

1. Introduction

Ultra-high performance fibre-reinforced concrete (UHPFRC) is a relatively new building material, which has superior durability, ductility and strength in comparison with Normal Strength Concrete (NSC) and Fibre Reinforced Concrete (FRC) [1–5]. Because of the superior characteristics of UHPFRC, much research has been conducted to investigate and enhance its static mechanical properties [6–8] and impact resistance capacity [9–15]. However, as sustainable development is currently a pressing global issue and various industries have strived to achieve energy savings. The high material cost, high energy consumption and embedded CO_2 for UHPFRC are the typical disadvantages that restrict its wider application [16–18]. Hence, how to produce a "green" UHPFRC remains an open question.

As commonly known, for the production of a high strength or ultra-high strength concrete matrix, a large amount of binder (around 1000 kg/m^3) is normally used [2–5,19]. To reduce the binder amount and produce a more cost effective UHPFRC, industrial by-products such as ground granulated blast-furnace slag (GGBS), fly ash (FA) and silica fume (SF) have been used as partial cement replacements in UHPFRC [2,3,19]. Moreover, some waste or recycled materials are included in the production of Ultra-high performance concrete (UHPC) or UHPFRC, such as rice husk ash [6,7], recycled glass cullet [8], palm oil fuel ash [20] and waste ceramics [21]. Another method to minimize the cost and environmental impact of UHPFRC is by reducing of the cement amount without sacrificing the mechanical properties. According to the previous experiences and investigations of the authors [22,75], by applying the modified Andreasen & Andersen particle packing model it is

* Corresponding author. Tel.: +31 (0) 40 247 5469; fax: +31 (0) 40 243 8595.
E-mail address: r.yu@tue.nl (R. Yu).

http://dx.doi.org/10.1016/j.conbuildmat.2014.06.033
0950-0618/

Nomenclature

d	diameter of the used fibres, mm
d_1	diameter of long steel fibres, mm
d_2	diameter of short steel fibres, mm
D_{max}	maximum particle size, μm
D_{min}	minimum particle size, μm
k	fibre embedded length, mm
K_f	hybrid fibre coefficient, –
K_t	strength improvement ratio, %
l	fibre length, mm
l_1	length of long steel fibres, mm
l_2	length of short steel fibres, mm
N_f	number of fibres embedded in the broken cross section, –
N_{f1}	number of long fibres embedded in the broken cross section, –
N_{f2}	number of short fibres embedded in the broken cross section, –
P_{mix}	composed mix, –
P_{tar}	target curve, –
q	distribution modulus, –
r	radius of the used fibres, mm
RSS	sum of the squares of the residuals, –
S_a	area of the broken cross section, mm^2
S_i	strength of the samples with fibres, N/mm^2
S_0	strength of the reference sample (without fibres), N/mm^2
U	total energy absorbed by the UHPHFRC sample, J
U_f	energy needed to pull out the fibre, J
U_{f1}	energy needed to pull out the long steel fibre, J
U_{f2}	energy needed to pull out the short steel fibre, J
U_m	crack energy absorbed by the reference sample (without fibres), J
U_Δ	modified total energy absorbed by the UHPHFRC samples, J
V_f	volumetric amount of the fibres in concrete, %
V_{f1}	volumetric amount of the long steel fibres, %
V_{f2}	volumetric amount of the short steel fibres, %
V_l	volumetric amount of long steel fibre, %
V_m	volume fraction of the matrix, %
V_s	volumetric amount of short steel fibre, %
W_{fp}	average work needed to pull out the fibre, J
x	fibre pulled out distance, mm
τ_i	interfacial frictional shear stress, N/mm^2

possible to produce a dense and homogeneous skeleton of UHPFRC with a relatively low binder amount (about 650 kg/m^3). However, from the available literature, research regarding the design or production of UHPFRC with an optimized particle packing is not sufficient [23–26]. In most cases, the UHPFRC recipes are given directly, without any detailed explanation or theoretical support. Hence, it can be predicted that a large amount of binders or other ingredients are not well utilized in UHPFRC, and the UHPFRC is not "green" enough.

Additionally, in comparison with the NSC, the application of UHPFRC is expected to improve the resistance capacity of construction and infrastructure under extreme mechanical or environmental loads, which should be mainly attributed to the contribution of fibres. The investigation regarding the effect of different fibres on the mechanical properties of UHPFRC can be readily found [3,27–30]. On the other hand, some studies focus on the reactions of UHPFRC under external impact loadings. For example, Millard [10], Mao [11], Wu [12], and Yi [31] investigated the blast-resistance characteristics of UHPFRC. Rong [13,14], Bragov [15], Caverzan [32], Tran [33] and Wang [34] presented the mechanical properties of UHPFRC under high strain rate loading. Nevertheless, all these studies did not consider the cost of utilized fibres, which is significant, since the cost of 1% volume content of fibre applied in UHPFRC is generally higher than that of the matrix [35]. Consequently, to achieve the goal of a "green" UHPFRC, it is important to minimize the amounts of fibres applied in UHPFRC without sacrificing its superior performance.

To efficiently utilize fibres in UHPFRC, one of the promising methods is to appropriately blend several different types of fibres in one concrete matrix [36,37]. There are many studies about the influence of hybrid fibres on the fresh and hardened properties of normal concrete [38–43]. Due to the fact that the short fibres can bridge the micro-cracks while the long fibres are more efficient in preventing the development of macro-cracks, the mechanical properties of hybrid fibre reinforced concrete can be better than that with only one type of fibre [42]. In recent years, the research focusing on the application of hybrid fibres in UHPFRC or influence of hybrid fibres on the properties of UHPFRC can also be found in the literature [5,35]. However, very little information is available about the dynamic behaviour of UHPFRC incorporating hybrid fibres, which may be attributed to the variation and complexity of the influence from hybrid fibres.

Following the path opened by foregoing studies, the aim of this research is to assess at a laboratory scale the static and dynamic properties of a "green" Ultra-High Performance Hybrid Fibre Reinforced Concrete (UHPHFRC). The design of concrete mixtures aims to achieve a densely compacted cementitious matrix with a relatively low binder amount, employing the modified Andreasen & Andersen particle packing model. The fracture mechanism of the UHPHFRC under impact loading is analyzed, and the modeling of the energy absorption capacity of UHPHFRC under impact loading is conducted.

2. Materials and methods

2.1. Materials

The cement used in this study is Ordinary Portland Cement (OPC) CEM I 52.5 R, provided by ENCI (the Netherlands). A polycarboxylic ether based superplasticizer is used to adjust the workability of concrete. Limestone powder is used as a filler to replace cement. A commercially available nano-silica in a slurry (AkzoNobel, Sweden) is applied as the pozzolanic material. Two types of sand are used, one is normal sand in the fraction of 0–2 mm and the other one is a micro-sand in the 0–1 mm size range (Graniet-Import Benelux, the Netherlands). The particle size distributions of the used granular materials are shown in Fig. 1. Additionally, two types of straight steel fibres are utilized (as shown in Fig. 2): (1) fibre length = 13 mm, fibre diameter = 0.2 mm; (2) fibre length = 6 mm, fibre diameter = 0.16 mm. The densities of the used materials are shown in Table 1.

2.2. Experimental methodology

2.2.1. Mix design of UHPHFRC

According to the previous investigation of the authors, it has already been demonstrated that it is possible to produce UHPFRC with relatively low binder amount [22]. Hence, in this study, the so-called modified Andreasen and Andersen model is utilized to design all the concrete mixtures, which is shown as follows [44,45]:

$$P(D) = \frac{D^q - D_{min}^q}{D_{max}^q - D_{min}^q} \quad (1)$$

where D is the particle size (μm), $P(D)$ is the fraction of the total solids smaller than size D, D_{max} is the maximum particle size (μm), D_{min} is the minimum particle size (μm) and q is the distribution modulus.

The modified Andreasen and Andersen packing model has already been successfully employed in optimization algorithms for the design of normal density concrete [46,49,50,76,77] and lightweight concrete [47,48]. Different types of con-

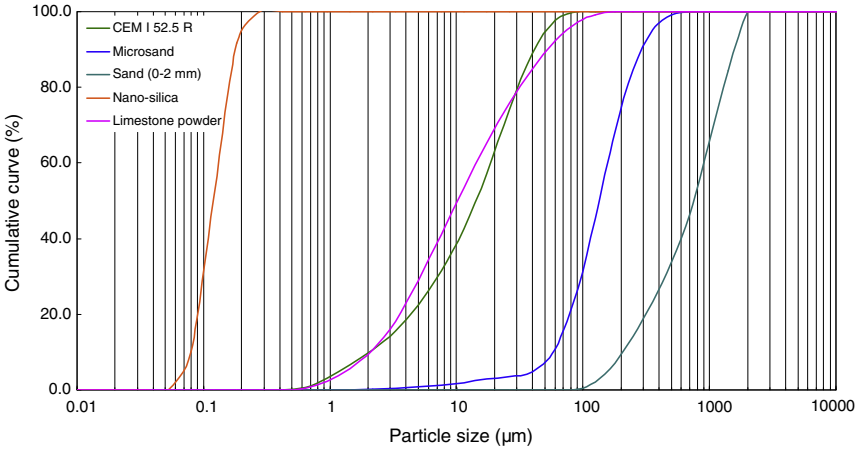

Fig. 1. Particle size distribution of the used concrete ingredients.

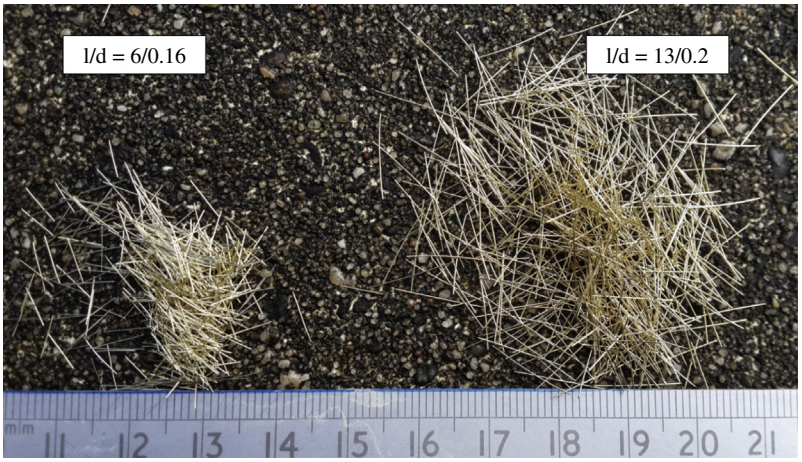

Fig. 2. Steel fibres used in this study.

Table 1
Information of materials used.

Materials	Type	Specific density (kg/m^3)
Cement	CEM I 52.5 R	3150
Filler	Limestone powder	2710
Fine sand	Micro-sand	2720
Coarse sand	Sand 0–2 mm	2640
Superplasticizer	Polycarboxylate ether	1050
Pozzolanic material	Nano-silica (nS)	2200
Fibre-1	Long steel fibre	7800
Fibre-2	Short steel fibre	7800

crete can be designed using Eq. (1) by applying different values of the distribution modulus q, as it determines the proportion between the fine and coarse particles in the mixture. Higher values of the distribution modulus ($q > 0.5$) lead to coarser mixtures, while lower values ($q < 0.25$) result in concrete mixes which are rich in fine particles [49]. Brouwers [50,51] demonstrated that theoretically a q value range of 0–0.28 would result in an optimal packing. Hunger [46] recommended using q in the range of 0.22–0.25 in the design of self-compacting concrete (SCC). Hence, in this study, considering that a large amount of fine particles are utilized to produce UHPHFRC, the value of q is fixed at 0.23, as recommended in [46].

In this research, the modified Andreasen and Andersen model (Eq. (1)) acts as a target function for the optimization of the composition of mixture of granular materials. The proportions of each individual material in the mix are adjusted until an optimum fit between the composed mix and the target curve is reached, using an optimization algorithm based on the Least Squares Method (LSM), as presented in Eq. (2). When the deviation between the target curve and the composed mix, expressed by the sum of the squares of the residuals (RSS) at defined particle sizes, is minimized, the composition of the concrete is considered optimal [52].

$$\mathrm{RSS} = \sum_{i=1}^{n} \left(P_{mix}(D_i^{i+1}) - P_{tar}(D_i^{i+1})\right)^2 \tag{2}$$

where P_{mix} is the composed mix, and the P_{tar} is the target grading calculated from Eq. (1).

Based on the optimized particle packing model, the developed UHPHFRC mixtures are listed in Table 2. The resulting integral grading curve of one mix is shown in Fig. 3 as an example. In this study, only about 620 kg/m^3 of binders is used to produce the "green" UHPHFRC, which is significantly lower than that reported in available literature [2–5]. For a typical normal fibre reinforced concrete, the fibre content is about 1% by the volume of concrete [53]. However, in UHPFRC, this value often increases to around 2 vol.%, and sometime reaches even 5 vol.% [53]. Hence, in this research, to investigate the effect of hybrid fibres on the properties of UHPFRC, the steel fibres are added into the mixes in the total amount of 2.0 vol.%, and the proportions of long and short steel fibres are shown in Table 2. Here, a new concept named "hybrid fibre coefficient" is proposed (Eq. (3)), representing the fraction of short steel fibres in the total fibre amount.

$$K_f = \frac{V_s}{V_s + V_l} \tag{3}$$

where K_f is the proposed "hybrid fibre coefficient", V_s is the volumetric amount of short steel fibres in the concrete mixture, and V_l represents the volumetric amount of long steel fibres in concrete.

2.2.2. Selection of the employed mix procedures

In this study, following the method shown in [22], the concrete matrix is well mixed with the hybrid steel fibres, and the compete production time is around 7 min and 30 s. Moreover, mixing is always executed under laboratory conditions with dried and tempered aggregates and powder materials. The room temperature while mixing and testing is constant at around 21 °C.

Table 2
Recipes of developed UHPHFRC.

No.	C (kg/m^3)	LP (kg/m^3)	M-S (kg/m^3)	N-S (kg/m^3)	nS (kg/m^3)	W (kg/m^3)	SP (kg/m^3)	LSF (vol.%)	SSF (vol.%)
1	594.2	265.3	221.1	1061.2	24.8	176.9	44.2	0	0
2	594.2	265.3	221.1	1061.2	24.8	176.9	44.2	2.0	0
3	594.2	265.3	221.1	1061.2	24.8	176.9	44.2	1.5	0.5
4	594.2	265.3	221.1	1061.2	24.8	176.9	44.2	1.0	1.0
5	594.2	265.3	221.1	1061.2	24.8	176.9	44.2	0.5	1.5
6	594.2	265.3	221.1	1061.2	24.8	176.9	44.2	0	2.0

C: Cement, LP: Limestone powder, M-S: Micro-sand, N-S: Normal sand (0–2 mm), nS: Nano-silica, W: Water, SP: Superplasticizer, LSF: Long steel fibre, SSF: Short steel fibre.

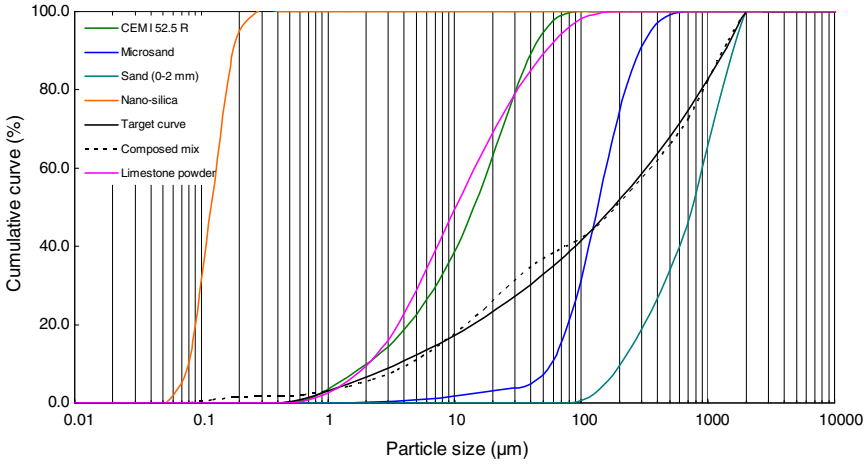

Fig. 3. PSDs of the concrete ingredients, target curve and resulting integral grading curve of the mixture.

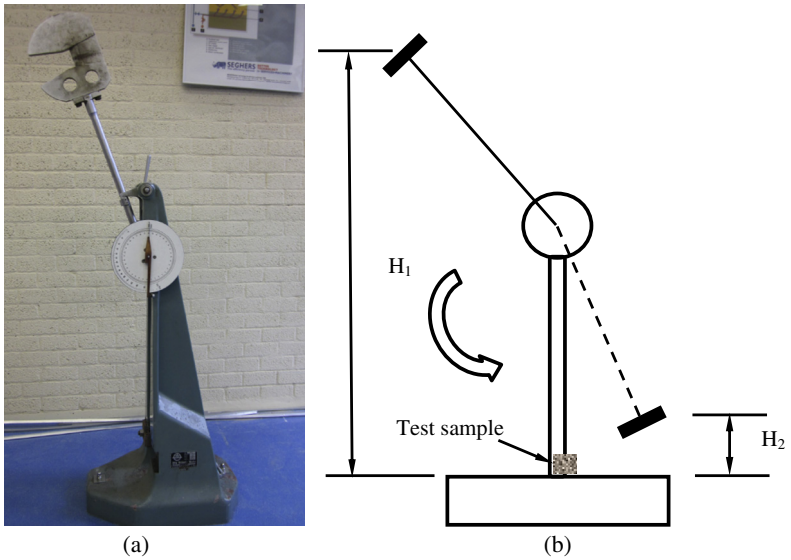

Fig. 4. Charpy impact test device used in this study (a) and its working scheme (b).

2.2.3. Workability of UHPHFRC

After the mixing, the fresh concrete is filled in a conical mould in the form of a frustum (as described in EN 1015-3 [54]). During the test, the cone is lifted straight upwards in order to allow free flow without any jolting. In the test, two diameters perpendicular to each other are determined. Their mean is recorded as the slump flow value of the designed UHPHFRC.

2.2.4. Static mechanical properties of UHPHFRC

After preforming the workability test, UHPHFRC is cast in moulds with the size of 40 mm × 40 mm × 160 mm and compacted on a vibrating table. The prisms are demoulded approximately 24 h after casting and subsequently cured in water at about 21 °C. After curing for 28 days, the prism specimens are tested under three-point loading using a testing machine controlled by an external displacement transducer, such that the mid-span deflection rate of the prism specimen is held constant throughout the test. The specimen mid-span deflection rate is set to 0.10 mm/min, with a span of 100 mm. Afterwards, the compressive strength test on the samples is executed according to the EN 196-1 [55]. During the testing, at least three specimens are tested for each batch.

2.2.5. Dynamic test of UHPHFRC

To evaluate the impact resistance capacity of concrete, many instruments can be utilized. In this study, the "Charpy impact test" is employed to test the energy absorption capacity of UHPHFRC, according to the ASTM E23 [56]. The Charpy impact device is shown in Fig. 4(a), in which the maximum kinetic energy output

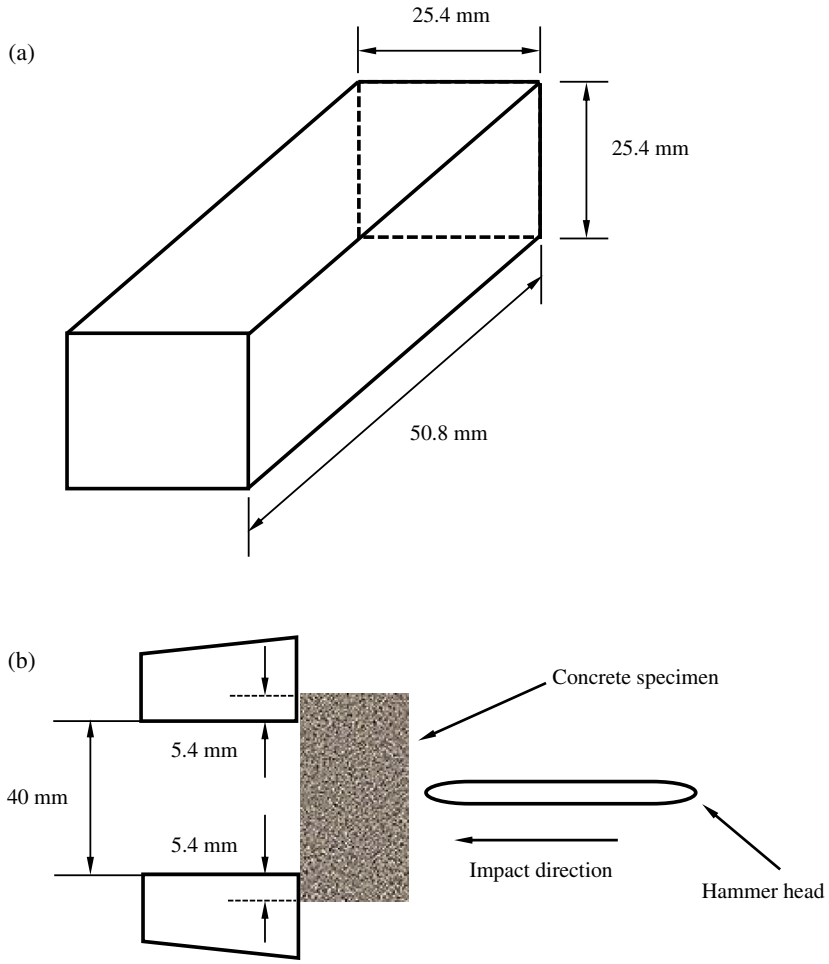

Fig. 5. Dimensions of specimen and the configuration of impact loading.

is 147.1 J. The dimension of the specimen and the configurations of the loading for the Charpy impact test are presented in Fig. 5 [57]. After embedding the specimen, the pendulum is released from a height H_1 and swing through the specimen to a height H_2, as shown in Fig. 4(b). Assuming negligible friction and aerodynamic drag, the energy absorbed by the specimen is equal to the height difference multiplied by the weight of the pendulum. During the testing, at least five specimens are tested for each batch.

3. Experimental results and discussion

3.1. Slump flow

The slump flow of fresh UHPHFRC mixes versus the hybrid fibre coefficient (K_f) is depicted in Fig. 6. The data illustrates the relationship between the proportions of long and short steel fibres and the workability of the fresh UHPHFRC. It is important to notice that with an increase of the hybrid fibre coefficient, the slump flow ability of UHPHFRC first linearly increases, and then sharply decreases. For example, when the hybrid fibre efficient is zero (2 vol.% long steel fibres), the slump flow is 28.8 cm, which slightly increases to around 30.0 cm when the hybrid fibre efficient grows to 0.75 (0.5 vol.% long steel fibres and 1.5 vol.% short steel fibres). This phenomenon implies that the addition of short steel fibres (increasing K_f) improves the workability of UHPHFRC. However, when all the long steel fibres are replaced by short steel fibres, the flowability of UHPHFRC sharply reduces. As shown in Fig. 6, when the hybrid fibre coefficient is 1 (2 vol.% short steel fibres), the slump flow of UHPHFRC is only about 28.3 cm, which is even lower than that of concrete with 2 vol.% long steel fibres.

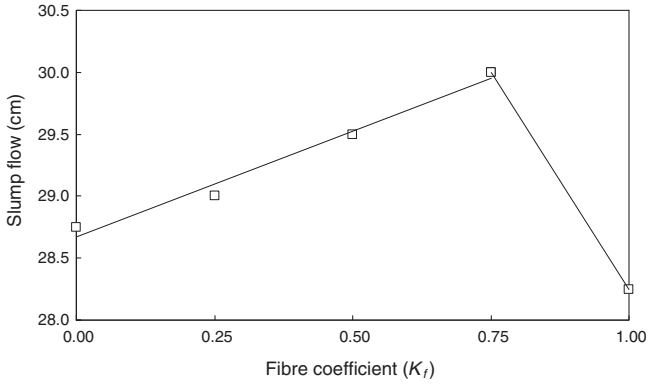

Fig. 6. Variation of the slump flow of UHPHFRC as function of the hybrid fibre coefficient (K_f).

As commonly known, the negative effect of steel fibres on the workability of concrete is mainly due to three reasons [53]: (1) The shape of the fibres is much more elongated compared with aggregates and the surface area at the same volume is higher, which can increase the cohesive forces between the fibres and the matrix; (2) Stiff fibres change the structure of the granular skeleton, and also push apart particles that are relatively large compared with the fibre length; (3) Steel fibres are often deformed (e.g. have hooked ends or are wave-shaped) to improve the anchorage between a fibre and the surrounding matrix. The friction

between hooked-end steel fibres and aggregates is higher compared with straight steel fibres. In this study, the hybrid fibres are utilized to produce the concrete, which means not only the above mentioned reasons, but also the mutual effects between the fibres should be considered. Based on the investigation by Boulekbache [58], it is known that different flow velocities affect the fibres and may cause them to rotate in such a way that the fibres reorient perpendicularly to the flow direction (Fig. 7). In the presence of relative velocities in translation and rotation, the fluid exerts forces and momentums on the fibres. Hence, for the fresh concrete with single type fibres, the entire fibre orientation tends to be perpendicular to the flow direction in the fountain flowing mode, which can generate the largest resistant force and reduce the slump flow of the fresh concrete. Nevertheless, when hybrid fibres are added into the fresh concrete, the fountain flowing mode may be relatively disturbed. When casting concrete in moulds, the fibres close to the walls of the moulds tend to be parallel to the borders, which is named the "wall-effect" [42,53]. Hence, in this study, when hybrid fibres are added into the fresh concrete, the long steel fibres can be treated as "imaginary borders" to the short steel fibres, and can relatively resist the rotation of the short fibres and reduce the resistance force in the fountain flow (Fig. 8). Furthermore, the short steel fibres can also conversely restrict the rotation of the long steel fibres and further improve the "wall-effect" of long steel fibres. Therefore, the flowability of the hybrid fibres reinforced concrete is larger than that with only one type of steel fibres.

3.2. Static mechanical properties

3.2.1. Flexural test results and analysis

The stress–strain curves of UHPHFRC during the flexural test at 7 and 28 days are shown in Fig. 9(a) and (b). Similarly to the results shown in the literature [6–8], the addition of steel fibres (2 vol.%) can not only enhance the ultimate flexural strength, but also improve the energy absorption capacity of the designed UHPHFRC. This should be attributed to the fact that the additional steel fibres can bridge cracks and retard their propagation, which could change the fracture behaviour of concrete from brittle to plastic and significantly increase the ultimate flexural strength of concrete [53]. Moreover, it is important to notice that the flexural properties of the specimen strongly depend on the fractions of the long and short steel fibres in the total fibre amount. As can be seen in Fig. 9, the ultimate flexural strengths of the concrete with long steel fibres (1.5 vol.%) and short steel fibres (0.5 vol.%) at 7 and 28 days are always the largest, which are 24.3 MPa and 30.9 MPa, respectively. When only short steel fibres are utilized (2 vol.%), the ultimate flexural strengths at 7 and 28 days reduce to around 18.4 MPa and 21.5 MPa, respectively. This can be explained by the following two reasons: (1) short fibres can bridge micro-cracks more efficiently, because they are very thin and their number in concrete is much higher than that of the long steel fibres, for the same fibre volume. Hence, when the micro-cracks are just generated in the concrete specimen, the short steel fibres can effectively bridge the micro-cracks. As the micro-cracks grow and merge into larger macro-cracks, the long steel fibres become more and more active in crack bridging. In this way, primarily the ductility can be improved, and partly also the flexural strength. Long fibres can therefore provide a stable post-peak response. Short fibres will then become less and less active, because they are being more and more pulled out, as the crack width increases [42]; (2) long fibres are always well oriented between the two imaginary borders, if casting of concrete in layers is applied (these borders may also be the walls of the moulds). With such positions, the long fibres form a kind of a barrier for short fibres, and limit their space for rotation. The short fibres will therefore be somewhat better oriented when combined together with long fibres, than on their own (Fig. 10) [42]. Hence, more fibres distribute in the direction parallel to the force direction in the flexural test, and the mechanical properties can be significantly improved. Additionally, for the

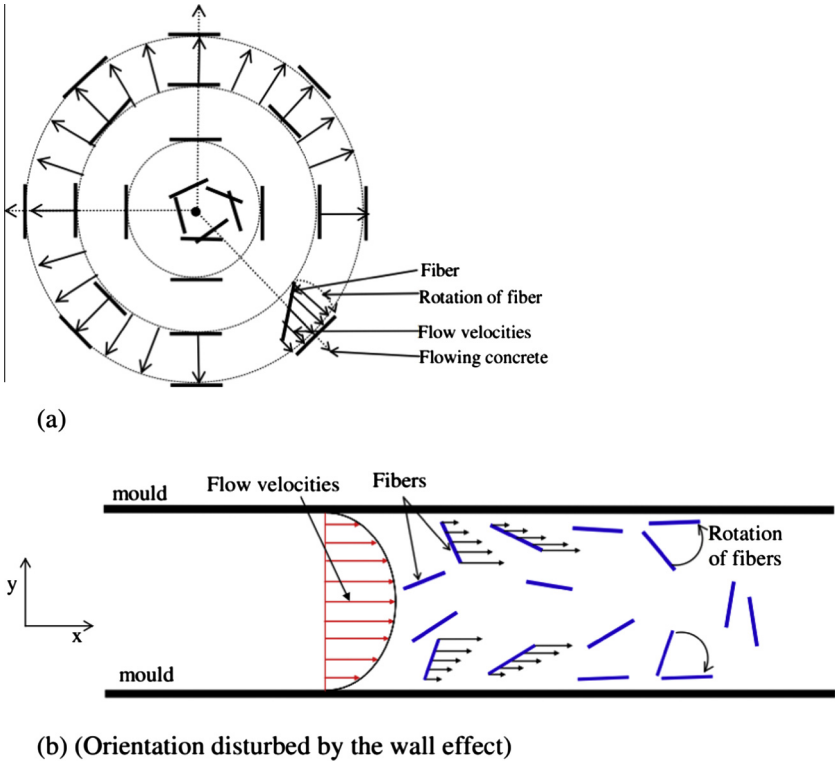

Fig. 7. Single type steel fibre orientations in (a) fountain flowing, and (b) canal channel flowing [58].

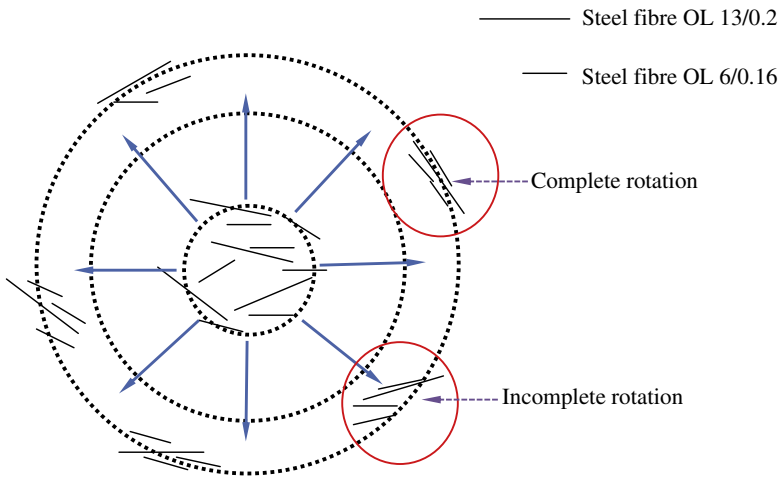

Fig. 8. Scheme of the influence from the imaginary "wall-effect" between the long and short steel fibres.

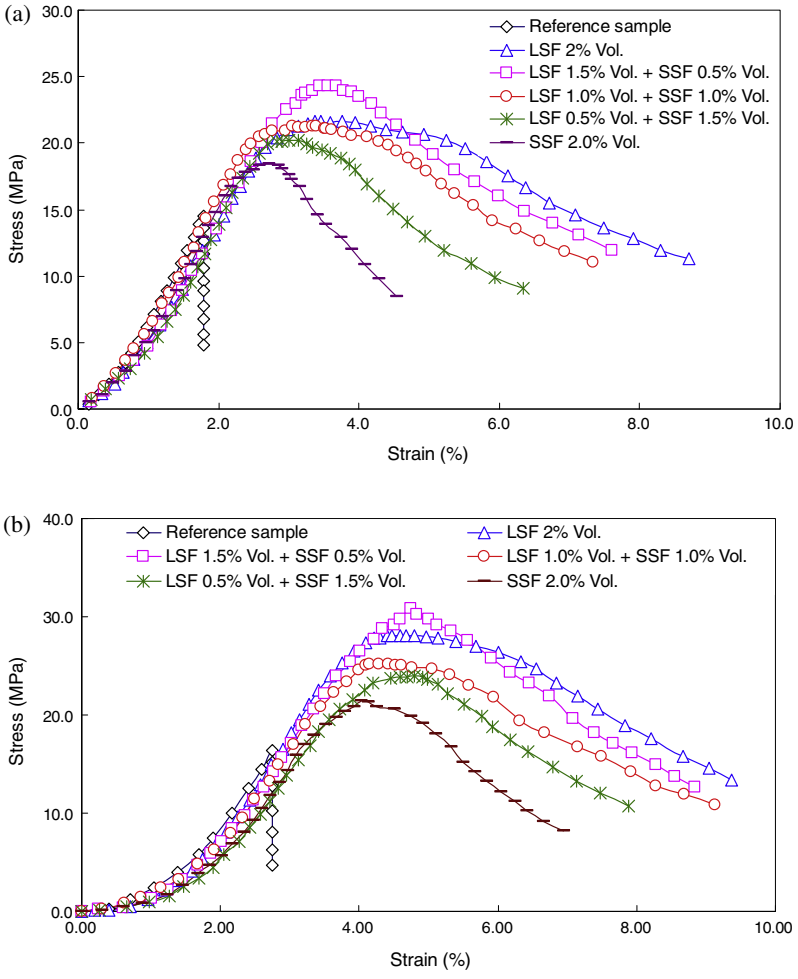

Fig. 9. Stress–strain curve of UHPHFRC under flexural test: (a) after curing for 7 days; and (b) after curing for 28 days.

sample with the largest ultimate flexural strength, it is important to notice that the stress quickly drops after reaching the stress peak. This should be attributed to the fact that the short steel fibres are less effective in bridging the macro-cracks and cannot provide a stable post-peak response. After calculating the area under the curves shown in Fig. 9, it is demonstrated that the energy absorption capacity of the batch with largest flexural strength may not be the largest, compared to the other mixtures in this research (161.4 units for reference sample and 139.8 units for LSF 1.5% Vol. + SSF 0.5% Vol. at 28 days).

In summary, the flexural properties of UHPHFRC largely depend on the proportions between the long and short steel fibres. In this

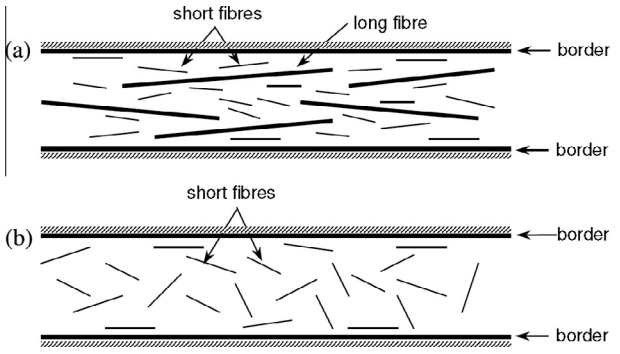

Fig. 10. Orientation of short fibres between the walls of the mould (or any other borders in general), in combination with long fibres (a), and when they are alone on their own (b) [42].

study, although the sample with long steel fibres (1.5 vol.%) and short steel fibres (0.5 vol.%) shows the largest ultimate flexural strength, its post-peak response is not the highest observed.

3.2.2. Compressive test results and analysis

The compressive strengths of the designed UHPHFRC with different hybrid fibre coefficients are presented in Fig. 11. As can be seen, compared to the reference sample, the additional steel fibres significantly increase the compressive strength of UHPHFRC. For instance, the compressive strengths of the reference sample (without steel fibres) at 7 and 28 days are 86.0 MPa and 99.0 MPa, respectively. When long steel fibres are added (2 vol.%) into the concrete, the compressive strength increase to about 114.3 MPa and 139.3 MPa after curing for 7 and 28 days, respectively. Moreover, similarly to the results shown in Fig. 9, the sample with long steel fibres (1.5 vol.%) and short steel fibres (0.5 vol.%) shows the largest compressive strengths, which are 117.1 MPa and 141.5 MPa after curing for 7 and 28 days, respectively. This should also be attributed to the combined effect of hybrid fibres in restricting the cracks development. Although the fibres are more efficient in improving the properties of concrete under tensile or flexural loads, they can also bridge the cracks that are generated in the compressive test and enhance the ultimate compressive strength of the concrete. However, it is important to notice that, when only short steel fibres are added into the concrete, the compressive strength slightly increases to 111.4 MPa and 120.8 MPa after 7 and 28 days, respectively. This should be attributed to the dimensions and aspect ratio of the short steel fibres. As shown in Fig. 2, the length of the short steel fibres used in this study is 6 mm, which is less efficient in restricting the growth of macro-cracks. Hence, the addition of short steel fibres (2 vol.%) is not as efficient as long steel fibres (2 vol.%) in improving the compressive strength of UHPHFRC.

The compressive strength results demonstrate that, based on the modified Andreasen & Andersen particle packing model, it is possible to produce UHPFRC with a relatively low cement or binder amount. The comparison of the binder amount and compressive strength (28 days) between the optimized and non-optimized UHPFRC is shown in Table 3. It is clear that, with a lower binder amount, the compressive strength of the optimized UHPFRC is still comparable to the non-optimized UHPFRCs, which have a higher amount of binder. For instance, in the results shown by Hassan [3], about 1200 kg/m^3 of binder is utilized to produce UHPFRC, and its compressive strength at 28 days is about 150 MPa. In this study, only about 620 kg/m^3 of binder is utilized in UHPHFRC, but its compressive strength can also reach around 142 MPa. Additionally, according to [50], the cement efficiency of the designed UHPHFRC matrix can be calculated, which is about 0.17 MPa/kg/m^3. Although this value is smaller than some of the Eco-concretes [46,52], it is much higher than that of other UHPCs [71–74]. Hence, it is confirmed here that the optimized UHPHFRC matrix can have significantly reduced binder amount (without sacrificing the mechanical properties) and be more "green" in the terms of cement amount.

3.2.3. Effect of hybrid fibres on the strengths improvement

To better explain the effect of the additional steel fibres on the flexural and compressive strengths improvement of UHPHFRC, the strength improvement ratio is computed as follows [59]:

$$K_t = \frac{S_i - S_0}{S_0} \times 100\% \quad (4)$$

where the K_t (%) is the strength improvement ratio, S_i (MPa) is the strength of the samples with fibres and S_0 (MPa) is the strength of the reference sample (without fibres).

The flexural and compressive strength improvement ratios of UHPHFRC versus the hybrid fibre coefficient (K_f) are illustrated in Fig. 12. It can be noticed that, for the flexural strength improvement ratio, with an increasing value of the hybrid fibre coefficient (K_f), the strength improvement ratio firstly increases, and then sharply decreases. For instance, when the hybrid fibre coefficient equals 0.25, the flexural strength improvement ratios are 48.9% and 70.1% at 7 and 28 days, which both drop about 30% when the hybrid fibre coefficient increases to 1. Moreover, the influence

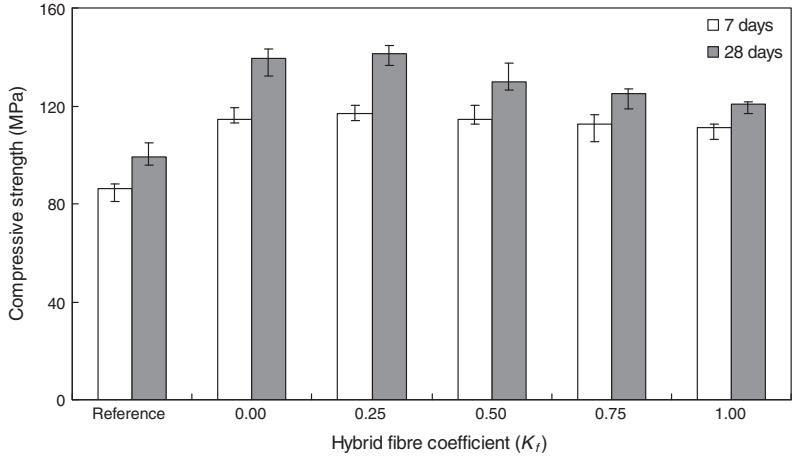

Fig. 11. Compressive strength of UHPHFRC with different hybrid fibre coefficients (K_f).

Table 3
Comparison of the binder amount and compressive strength (28 days) of optimized and non-optimized UHPFRC.

References	Binders (kg/m^3)			Water/binder ratio	Steel fibre amount (vol.%)	Compressive strength at 28 days (MPa)
	Cement	GGBS	Silica fume			
Yang [8]	950	0	238	0.20	2.0	190
Kang [27,28]	860	0	215	0.20	2.0	198
Hassan [3]	657	418	119	0.17	2.0	150
Yang [29]	657	430	119	0.15	2.0	120
Toledo Filho [23]	1011	0	58	0.15	2.0	160
Corinaldesi [69]	960	0	240	0.16	2.5	155
Habel [70]	1050	0	275	0.14	6.0	160
Optimized "green" UHPHFRC	594.2	0	24.8 (nano-silica)	0.20	2.0	142

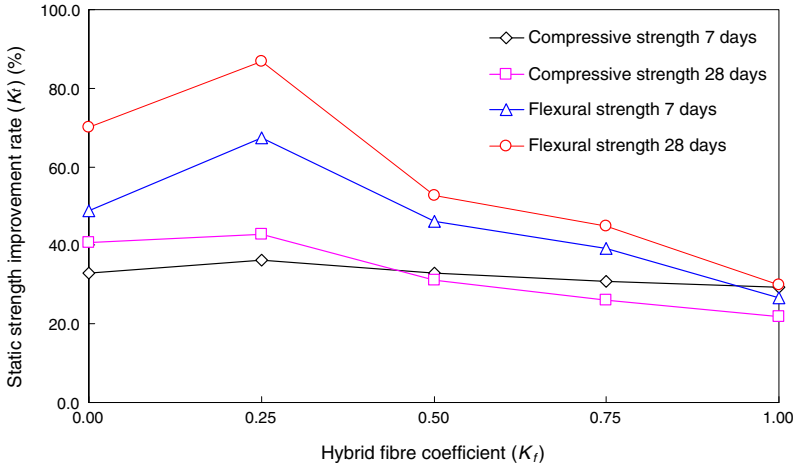

Fig. 12. Variation of the static strength improvement rate (K_t) of UHPHFRC with different hybrid fibre coefficients (K_f).

of the hybrid fibre coefficient on the compressive strength improvement ratio is relatively insignificant, and fluctuates in the range of 35–40%. This phenomenon also proves that the additional steel fibres are more efficient in improving the flexural properties. However, to enhance the efficiency of the utilized steel fibres, the hybrid design is preferable. In this study, the UHPHFRC with long steel fibre (1.5 vol.%) and short steel fibres (0.5 vol.%) shows the best fibre efficiency and best mechanical properties. This should be also attributed to the mutual effect of long and short steel fibres on the fibre distribution, which has already been explained in the previous part.

3.3. Dynamic properties of UHPHFRC

Fig. 13 shows the fractions of UHPHFRC and reference samples after the impact testing. It can be found from the experiments that the broken UHPHFRC samples are always composed of three cuboid-like fractions, while the fractions of reference samples are smaller and more irregular, as shown in Fig. 13(a). Moreover, after the impact on UHPHFRC samples, not only the concrete matrix is destroyed, but also all the embedded steel fibres are pulled out (Fig. 13(b)), which implies that the impact energy absorption of the UHPHFRC specimen should mainly include two parts: the energy used to break the concrete matrix and the energy used to pull out the fibres embedded in the broken cross sections.

As commonly known, the fracture mechanism of concrete under high strain rate or external impact loading should be attributed to cracking, shearing and compaction, as shown in Fig. 14 [60]. It can be predicted that concrete will be broken along the forces direction, such as compaction, tension or confining pressures. However, the final cracks development in the whole concrete element depends on the basic properties of the concrete, the addition of

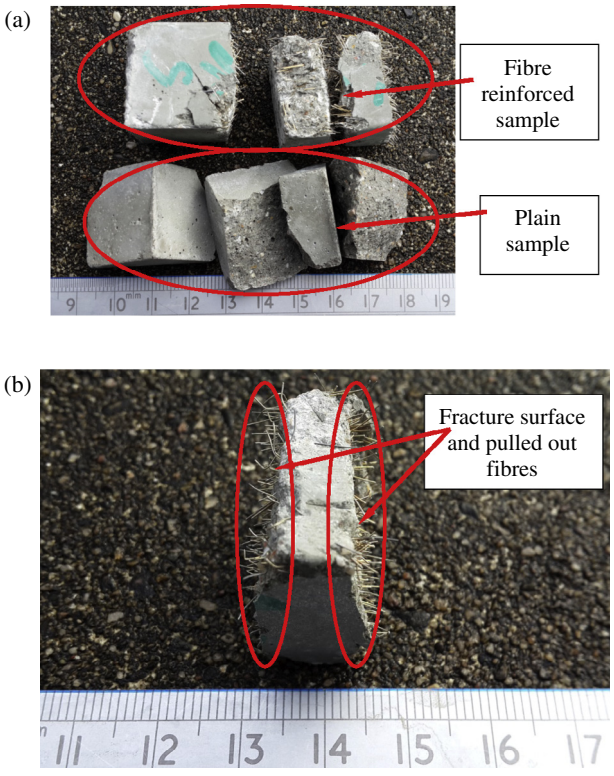

Fig. 13. Fractions of the samples after the Charpy impact test: (a) Comparison of the reinforced and non-reinforced sample after impact loading; and (b) Fractured surface of the reinforced sample after impact loading and the pulled out fibres.

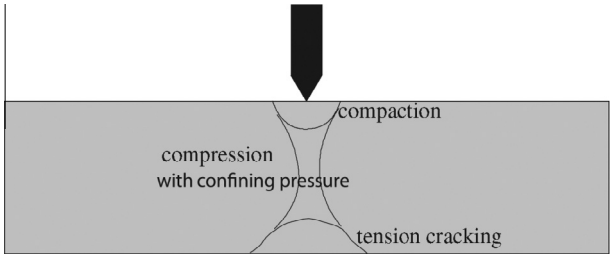

Fig. 14. Schematic description of the mechanisms activated in concrete under impact loading [60].

fibres or steel reinforcement. The numerical and experimental investigation of Süper [61] on thick concrete plates seems to show that when the first diagonal crack occurs, still a very high portion of the initial kinetic energy is transferred from the concrete to the reinforced steel, stirrups as well as longitudinal reinforcement. Hence, when the first crack occurs, the fibres can still bridge the crack and disperse the energy to other places in the concrete. Once the fibres can not restrict the development of cracks, they will be pulled out, and the concrete will be damaged following the stress distribution on concrete during the impact (Fig. 14). In this study, after performing the Charpy test, it has been observed that each concrete sample is broken mainly into three pieces, according to the stress distribution. Nevertheless, for non-reinforced concrete, due to the fact that no fibres or reinforcements can restrict the cracks development, the cracks always grow along the weakest interface in the concrete, which causes that the broken fractions of the reference sample are small and irregular (as shown in Fig. 13(a)).

To quantify the impact resistance capacity of concrete, the variation of the impact energy absorption of UHPHFRC with different hybrid fibre coefficients (K_f) is investigated, and is shown in Fig. 15. Note that with an increase of the value of the hybrid fibre coefficient, the impact energy absorption of UHPHFRC at 7 and 28 days decreases linearly. For instance, when the hybrid fibre coefficient increases from 0 to 1, the impact energy absorption of UHPHFRC reduces from about 45.6 J and 69.1 J to around 22.3 J and 28.4 J at 7 and 28 days, respectively. Furthermore, the slope of the decreasing line at 28 days is even larger than that at 7 days, which reflects that a further improvement of the impact energy absorption capacity of UHPHFRC after curing for 7 days significantly reduces with an increased value of the hybrid fibre coefficient. Hence, based on the obtained experimental results, it can be concluded that the long steel fibres play a dominant role in improving the impact resistance capacity of UHPHFRC. With a constant total steel fibre amount, the addition of short fibres can cause a significant decrease of the impact resistance capacity of UHPHFRC. Actually, this phenomenon is in accordance with the results presented in Fig. 9, in which the sample with long steel fibres (1.5 vol.%) and short steel fibres (0.5 vol.%) shows the largest ultimate flexural strength but instable post-peak response.

Hence, according to the obtained experimental results, it can be concluded that the long steel fibre is more important than the short steel fibre in improving the impact resistance capacity of UHPHFRC. However, to clearly understand the mechanism of energy absorption process of UHPHFRC under impact loading, the theoretical analysis and modeling are needed, and are presented in the next part.

3.4. Modeling of the energy absorption capacity of UHPHFRC

As has already been mentioned, to evaluate the impact energy absorption of the UHPHFRC samples, two parts should be mainly considered: the energy used to break the concrete matrix and the energy used to pull out the fibres embedded in the broken cross sections. According to the literature [62,63], the fibre pullout process usually consists of three processes: (1) fibre/matrix working together; (2) fibre/matrix debonding; (3) fibre/matrix sliding. In this study, the fibre/matrix interfacial shear strength is assumed equal to the equivalent shear bond strength. Hence, the total energy absorption of the sample during the impact testing can be simply expressed as [57]:

$$U = U_m V_m + N_f U_f \tag{5}$$

where U is the total energy absorbed by the UHPHFRC samples, U_m is the crack energy absorbed by the reference sample without fibres, V_m is the volume fraction of the matrix, N_f is the number of fibres embedded in the broken cross section and U_f is the energy per fibre that is need to be pulled out.

In this study, due to the fact that both the long and the short steel fibres are pulled out during the impact loading, the energy that is consumed for pulling out both fibre types should be considered individually. Assuming that the energies consumed in pulling long and short steel fibres are independent, Eq. (5) should be rewritten as follows:

$$U = U_m V_m + N_{f1} U_{f1} + N_{f2} U_{f2} \tag{6}$$

where N_{f1} and N_{f2} are the number of long and short fibres embedded in the broken cross section, respectively, U_{f1} and U_{f2} represent

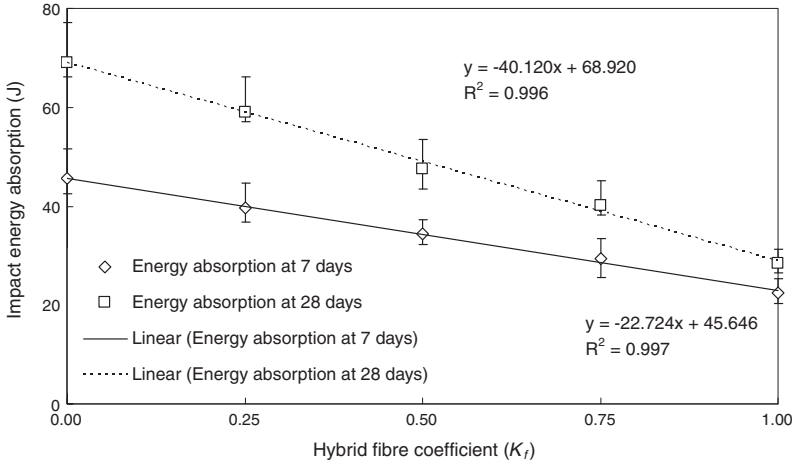

Fig. 15. Variation of the absorbed impact energy of UHPHFRC with different hybrid fibre coefficients (K_f).

the energy per long and short fibre that is needed to pull them out, respectively.

The fibre number can be computed as follows:

$$N_f = \frac{S_a V_f}{\pi r^2} = \frac{4 S_a V_f}{\pi d^2} \tag{7}$$

where S_a is the area of the broken cross section of the tested UHPHFRC samples, V_f is the volumetric amount of the fibres in concrete, r and d are the radius and diameter of the used fibres, respectively.

Additionally, in the literature [64–66] some investigations focusing on the estimation of the energy consumption in pulling out the embedded fibres can be found. Chawla [67] assumed that a fibre with a diameter d is pulled out through a distance x against an interfacial frictional shear stress (τ_i), then the total force at that instant on the debonded fibre surface opposing the pullout is $\tau_i \pi d (k–x)$, where k is the fibre embedded length. When the fibre is further pulled out a distance dx, the work done by this force is $\tau_i \pi d (k–x)\, dx$. The total work U_f done in pulling out the fibre over the distance k can be obtained by integration as follows [57]:

$$U_f = \int_0^k \tau_i \pi d \cdot (k - x) dx = \frac{\tau_i \pi d k^2}{2} \tag{8}$$

Here, assuming that the fibre cannot be broken during the pulling out process, its pullout length can vary between a minimum of 0 and a maximum of $l/2$, where l is the fibre length. Hence, integrating dk yields an average work of pullout per fibre, as follows [57]:

$$W_{fp} = \frac{1}{l/2} \int_0^{l/2} \frac{\tau_i \pi d k^2}{2} dk = \frac{\tau_i \pi d l^2}{24} \tag{9}$$

where W_{fp} is the average work of pullout per fibre.

So,

$$U_f = W_{fp} = \frac{\tau_i \pi d l^2}{24} \tag{10}$$

Now, these equations of are applied to the hybrid fibre reinforced concrete developed in this study. Substituting Eq. (10) and Eq. (7) into Eq. (6) gives:

$$U = U_m V_m + \frac{\tau_{i1} l_1^2 S_a V_{f1}}{6 d_1} + \frac{\tau_{i2} l_2^2 S_a V_{f2}}{6 d_2} \tag{11}$$

In order to calculate the total impact energy absorbed by the UHPHFRC from Eq. (11), it is necessary to obtain the interfacial bond strength between the concrete matrix and long or short steel fibres (τ_{i1} and τ_{i2}), which is defined as the friction between the fibre and the matrix [57]. The ultimate flexural stress in the mid-span can be expressed as the summation of the flexural stresses of the matrix and the fibres. Hence, the interfacial bond strength can be obtained as follows [57,68]:

$$\sigma = \frac{1}{2} \cdot V_f \cdot g \cdot \tau_i \cdot \left(\frac{L_f}{d_f}\right) + \sigma_m \cdot (1 - V_f) \tag{12}$$

where σ is the flexural stress of UHPHFRC, σ_m is the flexural stress of the reference sample with fibres, $g = 1.5$ [68].

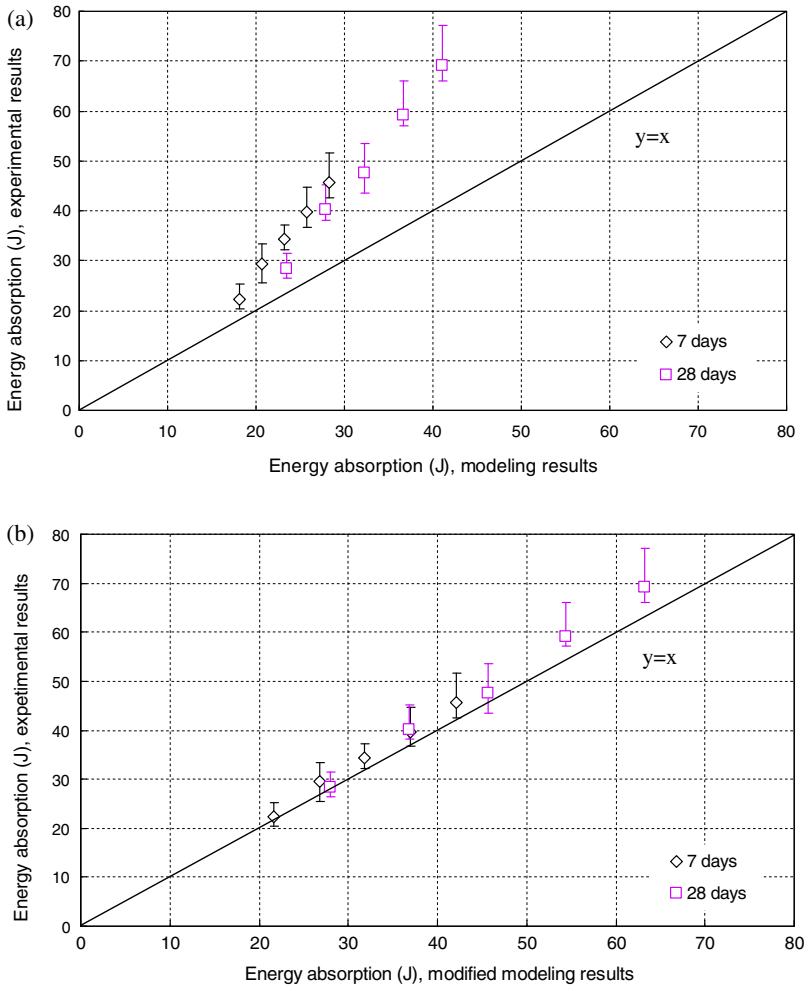

Fig. 16. Comparison of the experimental and modeling results of the energy absorption of UHPHFRC during the impact loading, (a) based on original model, and (b) based on the modified model.

Hence, applying the results shown in Fig. 9 and Eqs. (11) and (12), the energy absorbed by UHPHFRC during the impact can be computed. A comparison between the experimental and modeling results is presented in Fig. 16(a). It can be noticed that all the modeling results underestimate the experimentally measured energy absorption capacity of UHPHFRC. Especially for the concrete mixtures having higher impact resistance ability, the deviation between the experimental and modeling results is larger. Hence, to better represent the experimental results, the presented model needs further consideration.

As mentioned before, in this study, the impact energy absorption of UHPHFRC samples is mainly composed of two parts: the energy used to break the concrete matrix and the energy used to pull out the fibres embedded in the broken cross sections. Nevertheless, in the above modeling of the energy consumed on the pulling fibres out, only a single broken cross section is considered per sample. In fact, as can be seen in Fig. 13, after the impact loading, UHPHFRC is typically broken into three pieces, which means there are two broken cross sections and more energy is consumed in pulling out fibres. Consequently, here, we have proposed a new equation that gives the impact energy dissipation of a hybrid fibre reinforced concrete in the Charpy test. Assuming that the hybrid steel fibres are homogeneously distributed within the specimen, Eq. (11) is modified as follows:

$$U_{\Delta} = U_m V_m + 2 \cdot \left(\frac{\tau_{i1} l_1^2 S_a V_{f1}}{6 d_1} + \frac{\tau_{i2} l_2^2 S_a V_{f2}}{6 d_2} \right) \tag{13}$$

where U_{Δ} is the modified total energy absorbed by the UHPHFRC samples, l_1 and l_2 are the lengths of long and short steel fibres, d_1 and d_2 are the diameters of long and short steel fibres, V_{f1} and V_{f2} are the volumetric amounts of the long and steel fibres in UHPHFRC, respectively.

Based on the flexural stress testing results and Eqs. (12) and (13), the modified impact energy absorption of UHPHFRC can be calculated. The comparison between the experimental and modified modeling results is illustrated in Fig. 16(b). It is important to find that the modified modeling results are in good agreement with the experimental results, especially for the samples with lower energy absorption capacities. However, when the impact resistance ability of UHPHFRC is relatively high, the modeling results slightly underestimate the experimental results. This could be attributed to the fact that the energy absorbed in the test device vibration or the friction between the sample and the device is ignored in the modeling process. Actually, when the impact resistance capacity of the concrete is relatively high, small vibrations of the Charpy device could be observed indeed, which means that some part of the energy is dissipated in the equipment.

4. Conclusions

This article presents the analysis of the static and dynamic properties of a "green" Ultra-High Performance Hybrid Fibre Reinforced Concrete (UHPHFRC). From the results presented in this paper the following conclusions are drawn:

- By using the Andreasen & Andersen particle packing model, it is possible to produce a dense and homogeneous skeleton of UHPHFRC with a relatively low binder amount (about 620 kg/m^3), which can make the concrete more "green" and cost effective.
- With the same total steel fibre amount, the hybrid fibre reinforced concrete shows better workability than the one with a single type of fibres. This may be attributed to the fact that the long steel fibres can be treated as imaginary borders to the short steel fibres, which can relatively well restrict the rotation of the short fibres and reduce the resistance force in the fountain flow. Furthermore, the short steel fibres can also conversely restrict the rotation of the long steel fibres and further improve the "wall-effect" of the long steel fibres.
- Based on the static mechanical test results, it is found that the concrete with long steel fibres (1.5 vol.%) and short steel fibres (0.5 vol.%) shows the highest flexural and compressive strengths after curing for 28 days, which are 30.9 and 141.5 MPa, respectively. However, its flexural stress–strain curve more quickly decreases (compared to the reference sample) after reaching the peak stress, which implies that its energy absorption capacity slowly increases during the post-peak process.
- The dynamic impact test results show that the long steel fibre plays a dominating role in improving the impact resistance capacity of UHPHFRC. With a constant total steel fibre amount, the addition of short fibres can cause a decrease of the impact resistance capacity of UHPHFRC.
- A new equation is proposed to compute the energy dissipated in the hybrid fibre reinforced concrete for the Charpy test. The new model features a good correlation with the experimental results, especially for the samples with lower energy absorption capacity. When the impact resistance ability of UHPHFRC is relatively high, the modeling results slightly underestimate the experimental results (about 9.3%), which could be attributed to the energy dissipated into the test device.

Acknowledgements

The authors wish to express their gratitude to the colleagues G.A.H. Maas for his help with the impact tests experiments, to A.C.J. de Korte for his help in calculating the area under the curves shown in Fig. 9, to Dr. M.V.A. Florea for her editorial help in improving this manuscript and to the following sponsors of the Building Materials research group at TU Eindhoven: Graniet-Import Benelux, Kijlstra Betonmortel, Struyk Verwo, Attero, Enci, Provincie Overijssel, Rijkswaterstaat Zee en Delta - District Noord, Van Gansewinkel Minerals, BTE, V.d. Bosch Beton, Selor, Twee "R" Recycling, GMB, Schenk Concrete Consultancy, Geochem Research, Icopal, BN International, Eltomation, Knauf Gips, Hess ACC Systems, Kronos and Joma (CRH Europe Sustainable Concrete Centre, Cement & Beton Centrum and Heros in chronological order of joining).

References

[1] Richard P, Cheyrezy M. Composition of reactive powder concretes. Cem Concr Res 1995;25(7):1501–11.
[2] Tayeh BA, Abu Bakar BH, Megat Johari MA, Voo YL. Mechanical and permeability properties of the interface between normal concrete substrate and Ultra-high Performance Fibre concrete overlay. Constr Build Mater 2012;36:538–48.
[3] Hassan AMT, Jones SW, Mahmud GH. Experimental test methods to determine the uniaxial tensile and compressive behaviour of Ultra-high Performance Fibre Reinforced Concrete (UHPFRC). Constr Build Mater 2012;37:874–82.
[4] Rossi P. Influence of fibre geometry and matrix maturity on the mechanical performance of ultra-high-performance cement-based composites. Cem Concr Compos 2013;37:246–8.
[5] Park SH, Kim DJ, Ryu GS, Koh KT. Tensile behaviour of Ultra-High Performance Hybrid Fibre Reinforced Concrete. Cem Concr Compos 2012;34:172–84.
[6] Tuan NV, Ye G, Breugel K, Copuroglu O. Hydration and microstructure of ultra-high performance concrete incorporating rice husk ash. Cem Concr Res 2011;41:1104–11.
[7] Tuan NV, Ye G, Breugel K, Fraaij ALA, Dai BD. The study of using rice husk ash to produce ultra-high performance concrete. Constr Build Mater 2011;25:2030–5.
[8] Yang SL, Millard SG, Soutsos MN, Barnett SJ, Le TT. Influence of aggregate and curing regime on the mechanical properties of ultra-high performance fibre reinforced concrete (UHPFRC). Constr Build Mater 2009;23:2291–8.

[9] Katrin H, Paul G. Response of ultra-high performance fiber reinforced concrete (UHPFRC) to impact and static loading. Cem Concr Compos 2008;30:938–46.
[10] Millard SG, Molyneaux TCK, Barnett SJ, Gao X. Dynamic enhancement of blast-resistant ultra-high performance fibre-reinforced concrete under flexural and shear loading. Int J Impact Eng 2010;37:405–13.
[11] Mao L, Barnett S, Begg D, Schleyer G, Wight G. Numerical simulation of ultra-high performance fibre reinforced concrete panel subjected to blast loading. Int J Impact Eng 2013. http://dx.doi.org/10.1016/j.ijimpeng.2013.10.003.
[12] Wu C, Oehlers DJ, Rebentrost M, Leach J, Whittaker AS. Blast testing of ultra-high performance fibre and FRP-retrofitted concrete slabs. Eng Struct 2009;31:2060–9.
[13] Rong Z, Sun W, Zhang Y. Dynamic compression behavior of ultra-high performance cement based composites. Int J Impact Eng 2010;37:515–20.
[14] Rong Z, Sun W. Experimental and numerical investigation on the dynamic tensile behavior of ultra-high performance cement based composites. Constr Build Mater 2012;31:168–73.
[15] Bragov AM, Petrov YuV, Karihaloo BL, Konstantinov AYu, Lamzin DA, Lomunov AK, et al. Dynamic strengths and toughness of an ultra-high performance fibre reinforced concrete. Eng Fract Mech 2013;110:477–88.
[16] UNSTATS. Greenhouse gas emissions by sector (absolute values). United Nation Statistical Division: Springer; 2010.
[17] Friedlingstein P, Houghton RA, Marland G, Hackler J, Boden TA, Conway TJ, et al. Uptake on CO_2 emissions. Nat Geosci 2010;3:811–2.
[18] Habert G, Denarié E, Šajna A, Rossi P. Lowering the global warming impact of bridge rehabilitations by using ultra high performance fibre reinforced concretes. Cem Concr Compos 2013;38:1–11.
[19] El-Dieb AS. Mechanical, durability and microstructural characteristics of ultra-high-strength self-compacting concrete incorporating steel fibres. Mater Des 2009;30:4286–92.
[20] Aldahdooh MAA, Muhamad Bunnori N, Megat Johari MA. Development of green ultra-high performance fiber reinforced concrete containing ultrafine palm oil fuel ash. Constr Build Mater 2013;48:379–89.
[21] Vejmelková E, Keppert M, Rovnaníková P, Ondráček M, Keršner Z, Černy R. Properties of high performance concrete containing fine-ground ceramics as supplementary cementitious material. Constr Build Mater 2012;34:55–61.
[22] Yu R, Spiesz P, Brouwers HJH. Mix design and properties assessment of Ultra-High Performance Fibre Reinforced Concrete (UHPFRC). Cem Concr Res 2014;56:29–39.
[23] Toledo Filho RD, Koenders EAB, Formagini S, Fairbairn EMR. Performance assessment of Ultra-High Performance Fibre Reinforced Cementitious Composites in view of sustainability. Mater Des 2012;36:880–8.
[24] De Larrard F, Sedran T. Optimization of ultra-high-performance concrete by the use of a packing model. Cem Concr Res 1994;24:997–1009.
[25] De Larrard F, Sedran T. Mixture-proportioning of high-performance concrete. Cem Concr Res 2002;32:1699–704.
[26] Stark U, Mueller A, Optimization of packing density of aggregates. In: Proceedings of the second international symposium on ultra-high performance concrete. Kassel, Germany, March 05–07; 2008.
[27] Kang ST, Kim JK. The relation between fibre orientation and tensile behavior in an Ultra-High Performance Fibre Reinforced Cementitious Composites (UHPFRCC). Cem Concr Res 2011;41:1001–14.
[28] Kang ST, Kim JK. Numerical simulation of the variation of fibre orientation distribution during flow molding of Ultra-High Performance Cementitious Composites (UHPCC). Cem Concr Compos 2012;34:208–17.
[29] Yang IH, Joh C, Kim BS. Structural behavior of ultra-high performance concrete beams subjected to bending. Eng Struct 2010;32:3478–87.
[30] Sirijaroonchai K, El-Tawil S, Parra-Montesinos G. Behavior of high performance fibre reinforced cement composites under multi-axial compressive loading. Cem Concr Compos 2010;32:62–72.
[31] Yi NH, Kim JHJ, Han TS, Cho YG, Lee JH. Blast-resistant characteristics of ultra-high strength concrete and reactive powder concrete. Constr Build Mater 2012;28:694–707.
[32] Caverzan A, Cadoni E, Prisco M. Dynamic tensile behaviour of high performance fibre reinforced cementitious composites after high temperature exposure. Mech Mater 2013;59:87–109.
[33] Tran TK, Kim DJ. High strain rate effects on direct tensile behavior of high performance fiber reinforced cementitious composites. Cem Concr Compos 2014;45:186–200.
[34] Wang S, Zhang M, Quek S. Mechanical behavior of fiber-reinforced high-strength concrete subjected to high strain-rate compressive loading. Constr Build Mater 2012;31:1–11.
[35] Kim DJ, Park SH, Ryu GS, Koh KT. Comparative flexural behavior of Hybrid Ultra-High Performance Fiber Reinforced Concrete with different macro fibers. Constr Build Mater 2011;25:4144–55.
[36] Rossi P, Antonio A, Parant E, Fakhri P. Bending and compressive behaviors of a new cement composite. Cem Concr Res 2005;35(1):27–33.
[37] Rossi P. High performance multimodal fibre reinforced cement composite (HPMFRCC): the LCPC experience. ACI Mater J 1997;94(6):478–83.
[38] Ahmed SFU, Maalej M, Paramasivam P. Flexural responses of hybrid steel polyethylene fiber reinforced cement composites containing high volume fly ash. Constr Build Mater 2007;21(5):1088–97.
[39] Banthia N, Gupta R. Hybrid fiber reinforced concrete (HyFRC): fiber synergy in high strength matrices. Mater Struct 2004;37(10):707–16.
[40] Banthia N, Nandakumar N. Crack growth resistance of hybrid fiber reinforced cement composites. Cem Concr Compos 2003;25(1):3–9.
[41] Lawler JS, Wilhelm T, Zampini D, Shah SP. Fracture process of hybrid fiber reinforced mortar. Mater Struct 2003;35(3):197–208.
[42] Markovic I. High-performance hybrid-fibre concrete – development and utilisation. Technische Universität Delft, Ph.D. thesis; 2006.
[43] Yao W, Li J, Wu K. Mechanical properties of hybrid fiber-reinforced concrete at low fiber volume fraction. Cem Concr Res 2003;33(1):27–30.
[44] Andreasen AHM, Andersen J. Über die Beziehungen zwischen Kornabstufungen und Zwischenraum in Produkten aus losen Körnern (mit einigen Experimenten). Kolloid-Zeitschrift 1930;50:217–28 (In German).
[45] Funk JE, Dinger DR. Predictive process control of crowded particulate suspensions, applied to ceramic manufacturing. Boston, the United States: Kluwer Academic Publishers; 1994.
[46] Hunger M. An integral design concept for ecological self-compacting concrete. PhD thesis. Eindhoven University of Technology, Eindhoven, the Netherlands; 2010.
[47] Yu QL, Spiesz P, Brouwers HJH. Development of cement-based lightweight composites – Part 1: mix design methodology and hardened properties. Cem Concr Compos 2013;44:17–29.
[48] Spiesz P, Yu QL, Brouwers HJH. Development of cement-based lightweight composites – Part 2: durability related properties. Cem Concr Compos 2013;44:30–40.
[49] Hüsken G, Brouwers HJH. A new mix design concept for each-moist concrete: a theoretical and experimental study. Cem Concr Res 2008;38:1249–59.
[50] Brouwers HJH, Radix HJ. Self compacting concrete: theoretical and experimental study. Cem Concr Res 2005;35:2116–36.
[51] Brouwers HJH. Particle-size distribution and packing fraction of geometric random packings. Phys Rev E 2006;74:031309-1–031309-14.
[52] Hüsken G. A multifunctional design approach for sustainable concrete with application to concrete mass products. PhD thesis. Eindhoven University of Technology, Eindhoven, the Netherlands; 2010.
[53] Grünewald S. Performance-based design of self-compacting fibre reinforced concrete. Delft, the Netherlands: Delft University of Technology; 2004.
[54] BS-EN-1015-3. Methods of test for mortar for masonry – Part 3: Determination of consistence of fresh mortar (by flow table). British Standards Institution-BSI and CEN European Committee for Standardization; 2007.
[55] BS-EN-196-1. Methods of testing cement – Part 1: Determination of strength. British Standards Institution-BSI and CEN European Committee for Standardization; 2005.
[56] ASTME23, Standard test methods for notched bar impact testing of metallic materials. American Society for Testing and Materials; 1992.
[57] Xu B, Toutanji HA, Gilbert J. Impact resistance of poly (vinyl alcohol) fiber reinforced high-performance organic aggregate cementitious material. Cem Concr Res 2010;40:347–51.
[58] Boulekbache B, Hamrat M, Chemrouk M, Amziane S. Flowability of fibre-reinforced concrete and its effect on the mechanical properties of the material. Constr Build Mater 2010;24:1664–71.
[59] Pu XC. Super high strength and high performance concrete. China: Chongqing University Press; 2004.
[60] Burlion N. Compaction des betons: elements de modelisation et caracterisation experimentale. PhD dissertation, LMT, ENS de Cachan, France; 1997.
[61] Süper W. Rechnerische Untersuchung stoßartig beansprucher stahlbetonplatten. Lehrstuhl für Beton-und stahlbetonbau: Forschg. Kolloquim Dortmund; 1980.
[62] Favre JP, Désarmot G, Sudre O, Vassel A. Were McGarry or Shiriajeva right to measure glass–fiber adhesion? Compos Interfaces 1997;4:313–26.
[63] Kanda T, Li VC. Interface property and apparent strength of high-strength hydrophilic fiber in cement matrix. J Mater Civil Eng 1998;10:5–13.
[64] Leung CKY, Geng Y. Effect of lateral stresses on fiber debonding/pull-out. Compos Eng 1995;5(10):1331–48.
[65] Soetens T, Gysel AV, Taerwe ML. A semi-analytical model to predict the pull-out behaviour of inclined hooked-end steel fibres. Constr Build Mater 2013;43:253–65.
[66] Alwan JM, Naaman AE, Hansen W. Pull-out work of steel fibers from cementitious composites: analytical investigation. Cem Concr Compos 1991;13(4):247–55.
[67] Chawla KK. Composite materials science and engineering. New York: Springer-Verlag; 1997. p. 234–6.
[68] Kanda T, Li VC. Practical design criteria for saturated pseudo strain hardening behavior in ECC. J Adv Concr Technol 2006;4(1):59–72.
[69] Corinaldesi V, Moriconi G. Mechanical and thermal evaluation of Ultra-High Performance Fiber Reinforced Concretes for engineering applications. Constr Build Mater 2012;26:289–94.
[70] Habel K, Viviani M, Denarié E, Brühwiler E. Development of the mechanical properties of an Ultra-High Performance Fiber Reinforced Concrete (UHPFRC). Cem Concr Res 2006;36(7):1362–70.
[71] Deeb R, Ghanbari A, Karihaloo BL. Development of self-compacting high and ultra-high performance concretes with and without steel fibres. Cem Concr Compos 2012;34:185–90.
[72] Wang C, Yang C, Liu F, Wan C, Pu X. Preparation of Ultra-High Performance Concrete with common technology and materials. Cem Concr Compos 2012;34:538–44.
[73] Zhao S, Fan J, Sun W. Utilization of iron ore tailings as fine aggregate in ultra-high performance concrete. Constr Build Mater 2014;50:540–8.
[74] Yazici H. The effect of curing conditions on compressive strength of ultra high

strength concrete with high volume mineral admixtures. Build Environ 2007;42:2083–9.
[75] Yu R, Tang P, Spiesz P, Brouwers HJH. A study of multiple effects of nano-silica and hybrid fibres on the properties of Ultra-High Performance Fibre Reinforced Concrete (UHPFRC) incorporating waste bottom ash (WBA). Constr Build Mater 2014;60:98–110.
[76] Yu R, Spiesz P, Brouwers HJH. Effect of nano-silica on the hydration and microstructure development of Ultra-High Performance Concrete (UHPC) with a low binder amount. Constr Build Mater 2014;65:140–50.
[77] Quercia G, Spiesz P, Hüsken G, Brouwers HJH. SCC modification by use of amorphous nano-silica. Cem Concr Compos 2014;45:69–81.